Assessment of Climatology and Predictability of Mid-Atlantic Tropical Cyclone Landfalls in a High-Atmospheric-Resolution Seasonal Prediction System

JULIA V. MANGANELLO, BENJAMIN A. CASH, ERIK T. SWENSON, AND JAMES L. KINTER III

Center for Ocean–Land–Atmosphere Studies, George Mason University, Fairfax, Virginia

(Manuscript received 11 April 2019, in final form 24 May 2019)

ABSTRACT

Tropical cyclone (TC) landfalls over the U.S. mid-Atlantic region, which include the so-called Sandy-like, or westward-curving, tracks, are among the most infrequent landfalls along the U.S. East Coast. However, when these events do occur, the resulting economic and societal consequences can be devastating. A recent example is Hurricane Sandy in 2012. Multimodel ensemble seasonal hindcasts conducted with a high-atmospheric-resolution coupled prediction system based on the ECMWF operational model (Project Minerva) are used here to compile the statistics of these rare events. Minerva hindcasts are found to exhibit skill in reproducing climatological characteristics of the mid-Atlantic TC landfalls particularly at the highest atmospheric horizontal spectral resolution of T1279 (16-km grid spacing). Historical forecasts are further interrogated to identify regional and large-scale environmental conditions associated with these rare TC tracks to better quantify their predictability on synoptic time scales, and their dependence on model resolution. Evolution of the large-scale atmospheric flow patterns leading to mid-Atlantic TC landfalls is analyzed using local finite-amplitude wave activity (LWA). We have identified large-amplitude quasi-stationary features in the LWA and sea surface temperature (SST) anomaly distributions that persist up to about a week leading to these land-falling events. A statistical model utilizing indices based on the LWA and SST anomalies as predictors is developed that exhibits skill (mostly at T1279) in predicting mid-Atlantic TC landfalls several days in advance. Implications of these results for longer time-scale predictions of mid-Atlantic TC landfalls including climate change projections are discussed.

1. Introduction

Tropical cyclones (TC) are among the gravest natural hazards causing large human and material losses in many parts of the world. Over the recent period of record, more than 60% of all economic losses from these events [about $400 billion (U.S. dollars)] are due to North Atlantic TCs (e.g., Woodruff et al. 2013). In fact, the distribution of the damage and frequency of U.S. billion dollar weather and climate disasters is dominated by TC losses (Smith and Katz 2013). TC landfalls[1] over the mid-Atlantic region (specified here as the coastlines of Virginia, Chesapeake Bay, Delmarva Peninsula, and New Jersey) include the late recurving systems like Hurricanes Bertha (1996) and Floyd (1999) and the so-called Sandy-like, or westward-curving, tracks (see sections 2c and 2d and Fig. 1). These TC landfalls are among the most infrequent landfalls along the U.S. East Coast (e.g., Tolwinski-Ward 2015). However, when these events do occur, the resulting economic and societal consequences can be devastating. A recent example is Hurricane Sandy in 2012, which is considered the fourth-costliest[2] cyclone to hit the United States since 1900 (NHC 2018) with the greatest number of U.S. TC-related direct fatalities in the northeast since 1972 (Blake et al. 2013). In addition, the rate of sea level rise in the region is among the highest along the U.S. coasts [see Fig. 2 in Tebaldi et al. (2012)]. This factor along with the projected increase in TC intensities and the increase of coastal populations and infrastructure

[1] We consider landfalls by storms that are classified as tropical cyclones at some point in their life cycle and not necessarily at the time of landfall.

Supplemental information related to this paper is available at the Journals Online website: https://doi.org/10.1175/MWR-D-19-0107.s1.

Corresponding author: Julia V. Manganello, jvisneva@gmu.edu

[2] After Hurricane Katrina (2005), Hurricane Harvey (2017), and Hurricane Maria (2017).

DOI: 10.1175/MWR-D-19-0107.1

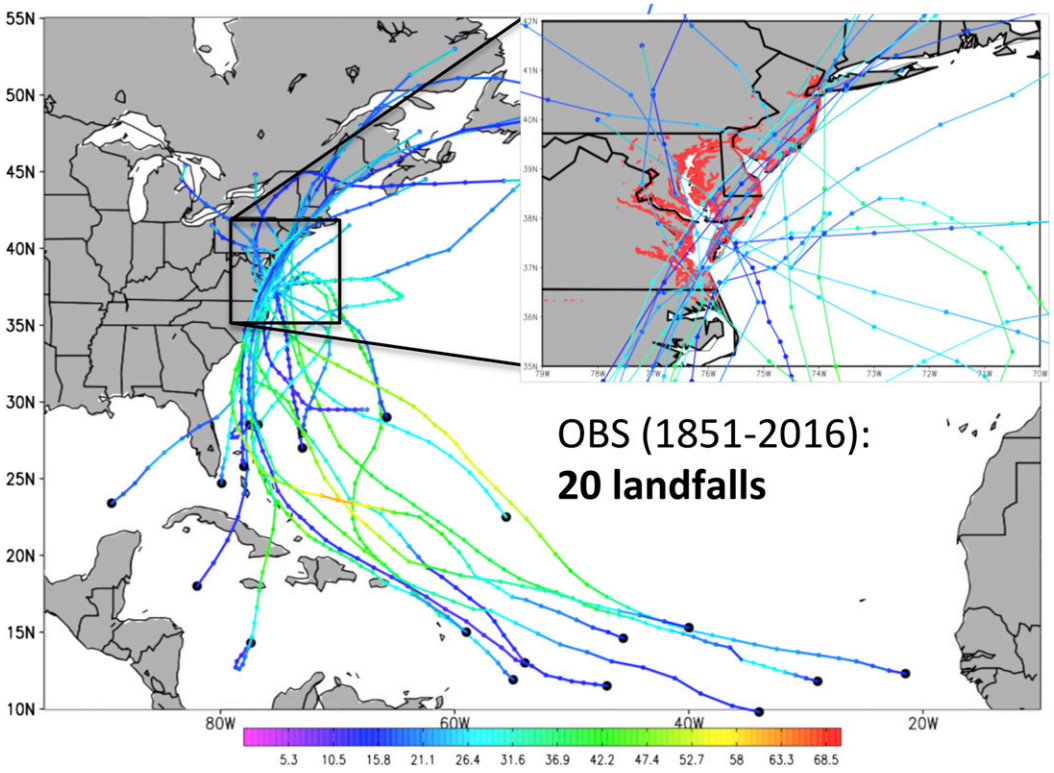

FIG. 1. Observed TC tracks (in 6-hourly segments) with landfalls in the mid-Atlantic during 1851–2016 identified according to the definitions in sections 2c and 2d. Color along the track represents the values of the 10-min MSW (see horizontal bar; scale is m s^{-1}). Genesis locations are shown in black filled circles. Mid-Atlantic coastline is shown in red in the inset.

would potentially lead to more damage from these land-falling events in the future (e.g., Wu et al. 2002; Lin et al. 2012; Woodruff et al. 2013).

An empirical analysis of mid-Atlantic TC landfalls is strongly limited by the fact that there are very few occurrences of these events in the observational record (see section 2d). Most previous studies on the subject have performed statistical-deterministic downscaling (Emanuel et al. 2006; Emanuel et al. 2008) or statistical-stochastic modeling (e.g., Hall and Jewson 2007) of the North Atlantic TCs, with a focus on the occurrence rate of Sandy-like tracks (Hall and Sobel 2013), the associated impacts (e.g., Reed et al. 2015; Lin et al. 2016) and the climate sensitivity of geographic landfall rates (Hall and Yonekura 2013). Climate change influences on large-scale atmospheric and oceanic conditions accompanying Sandy-like tracks have also drawn attention (e.g., Barnes et al. 2013; Lackmann 2015; Lau et al. 2016). In this study, we have utilized multimodel ensemble seasonal forecasts conducted with a high-atmospheric-resolution coupled prediction system (EPS; Project Minerva; Zhu et al. 2015; Cash et al. 2017) to compile the statistics of mid-Atlantic TC landfalls. State-of-the-art high-resolution EPSs have been recently shown to achieve reasonable skill in predicting seasonal TC activity on the regional scales (e.g., Vecchi et al. 2014; Camp et al. 2015; Manganello et al. 2016). Here, we further demonstrate that Minerva retrospective forecasts exhibit skill in reproducing basic statistics and climatological characteristics of mid-Atlantic TC landfalls particularly at the highest atmospheric horizontal spectral resolution of T1279 (16-km grid spacing).

Although dynamical ensemble forecasts may not produce as many land-falling events as the downscaling methods (mostly due to computational constraints) and may be prone to model errors, they have one distinct advantage that we capitalize upon. Since TCs are simulated explicitly in an EPS and evolve within a global synoptic environment, regional and large-scale environmental conditions associated with these rare TC landfalls can be identified and in turn their predictability and its limits, and the dependence on model resolution can be quantified. In addition, downscaling methods may not properly handle dynamical interactions with extratropical systems (Emanuel et al. 2006), which often occur during extratropical transition that many TCs at these high latitudes undergo. In fact, the westward hook or bend of a TC track during the extratropical transition is a

characteristic feature of strong midlatitude trough interaction (Fogarty and Blake, 2013). Downscaling methods may also be less accurate in regions with little historical data.

Furthermore, the evolution of the atmospheric flow patterns leading to the mid-Atlantic TC landfalls is analyzed here using local finite-amplitude wave activity (LWA), which has been shown to be an effective diagnostic of weather extremes at the regional scales, and which captures the local wave amplification associated with the blocking episode during Hurricane Sandy (Chen et al. 2015; Huang and Nakamura, 2016). We have identified large-amplitude quasi-stationary features in the LWA anomaly distribution that persist up to roughly a week prior to these land-falling events. We then introduce an index by averaging LWA anomalies over the selected regions and several days prior to landfall and develop a statistical model utilizing this index as a predictor, which is further shown to exhibit skill in predicting mid-Atlantic TC landfalls several days in advance. The implications of these results on longer time-scale predictions of these events including climate change projections are discussed.

The manuscript is organized as follows. Section 2 describes numerical experiments, methodologies of identifying and tracking TCs including mid-Atlantic TC landfall definition, and observational data. Basic statistics and climatological characteristics of land-falling TCs are described in section 3. Predictability of mid-Atlantic TC landfalls in Minerva is evaluated in section 4, and a corresponding statistical model is developed and assessed in section 5. A summary of the results and concluding remarks are given in section 6.

2. Data and methods

a. Numerical experiments

Ensemble seasonal hindcasts used here are performed with the Minerva forecasting system, which is an experimental EPS based on the ECMWF System 4 [see Manganello et al. (2016) for full details]. The ocean component model is the Nucleus for European Modeling of the Ocean (NEMO; Madec 2008) version 3.0, with the ORCA1 grid, which has a horizontal resolution of about 1° (with equatorial refinement of 1/3°) and 42 levels in the vertical. The atmospheric component model is the ECMWF Integrated Forecasting System (IFS; European Centre for Medium-Range Weather Forecasts 2013), cycle 38r1, which is a spectral, semi-implicit, semi-Lagrangian hydrostatic model with 91 levels in the vertical, and a model top in the mesosphere at 0.01 hPa. The IFS is integrated at spectral T319, T639, and T1279 horizontal resolutions, corresponding approximately to 62-, 31-, and 16-km grid spacing, respectively. These experiments are in turn referred to as T319, T639, and T1279 hereafter.

TABLE 1. TC identification criteria.

	Horizontal resolution of the Minerva forecasting system		
	T1279	T639	T319
1. Surface (10 m) wind speed threshold ($m\,s^{-1}$) (intensity threshold)	15.4[a]	14.4[a,b]	13.4[a,b]
2. Difference in vorticity[c] between 850 and 250 hPa (a warm core condition)	Larger than zero for all resolutions		
3. Vorticity[c] max at each level (6 levels) between 850 and 250 hPa (a coherent vertical structure condition)	Applied to all resolutions		
4. Criteria 1–3 are achieved for four consecutive time steps (24 h)	Applied to all resolutions		
5. Cyclogenesis (first identification) occurs between 0°–20°N over land and 0°–30°N over oceans	Applied to all resolutions		

[a] Observed "tropical storm" threshold for 10-min maximum sustained wind (MSW) is used.
[b] Surface wind speed threshold is further adjusted for model resolution based on Fig. 2 in Walsh et al. (2007). Values derived from a selection of Hurricane Research Division (HRD) wind analysis are used.
[c] Vorticity is truncated at T319 (N160) common to all resolutions.

Minerva retrospective forecasts are initialized on 1 May during 1980–2013 (1980–2012 for T319), are of 7-month duration and consist of 15 ensemble members for T1279 and T639 and 51 members for T319. This effectively represents 510 May–November (MJJASON) seasons for T1279 and T639, and 1683 seasons for T319. Upper-air data are truncated at spectral T21 resolution to remove the storm spatial scale (~1000 km; see, e.g., Manganello et al. 2014). This data are available only for T1279 and T319 (15 ensemble members).

b. Identification and tracking of tropical cyclones

Simulated storms are identified explicitly in the model databased on the tracking algorithm of Hodges (1994, 1995, 1999). Vortices are detected as maxima (in the Northern Hemisphere) in the 6-hourly relative vorticity field averaged between 850- and 600-hPa levels, with values greater than $5 \times 10^{-6}\,s^{-1}$ (at a spectral resolution of T63). To extract TCs from the raw tracks, a post-tracking lifetime filter of 2 days and a set of TC identification criteria (see Table 1) are applied. The latter include a 1) 10-m wind speed (intensity) threshold equivalent to the observed tropical storm intensity adjusted for model resolution for T639 and T319, 2) warm core condition, 3) coherent vertical structure condition,

TABLE 2. Basic statistics of mid-Atlantic TC landfalls from observations (IBTrACS) and Minerva hindcasts. All results are for the MJJASON season.

	IBTrACS		T1279 (1980–2013; 15 ensembles) (510 seasons)	T639 (1980–2013; 15 ensembles) (510 seasons)	T319 (1980–2012)	
	1851–2016 (166 seasons)	1900–2016[a] (117 seasons)			15 ensembles (495 seasons)	51 ensembles (1683 seasons)
Average rate (yr^{-1})	0.12	0.10	0.10	0.09	0.09	0.09
Average return period (yr)	8	10	10	11	11	11
Probability of landfall[b]	11%	10%	9%	9%	9%	9%
Probability of landfall in the next 10 seasons	72%	66%	64%	61%	63%	61%

[a] Starting 1900, the undercount bias in landfall counts along the coast of the U.S. is minimal (Landsea et al. 2004).
[b] Probability of landfall of one or more TCs based on the Poisson distribution. Differences between the model and observational values are statistically insignificant (at 95% confidence limit) using a Z test based on a joint Poisson distribution (see Tartaglione et al. 2003).

4) duration requirement for the above where the criteria 1–3 need to be jointly attained for at least four consecutive time steps (24 h) at some point during the life cycle of a storm, and 5) geographic extent of the cyclogenesis (first identification). As a result, model storms tend to include both earlier (precursor) and later (postextratropical transition) stages of a life cycle than the observed storms. Further details on the TC identification and tracking are provided in Manganello et al. (2016) and can also be found in Hodges et al. (2017).

c. *Definition of mid-Atlantic tropical cyclone landfalls*

The Northeast region of the United States is overall less vulnerable to direct strikes from TCs compared to the other parts of the U.S. East Coast due to the orientation of the coastline relative to the typical paths of the storms. These paths in the western North Atlantic are mostly northward and then northeastward in midlatitudes. To emphasize this point, we define the mid-Atlantic region as comprising the coastlines of Virginia, Chesapeake Bay, Delmarva Peninsula, and New Jersey (Long Island is therefore excluded as it is oriented roughly perpendicular to the mean TC tracks in the region and hence more vulnerable than the rest of the coastline).

For the above reasons, most TC landfalls (sea-to-land transitions) in the mid-Atlantic occur at a grazing impact angle unless the tracks exhibit a westward hook or bend, as is the case with Hurricane Sandy. In fact, Hurricane Sandy's near-perpendicular landfall on the New Jersey coast is found to be extremely rare (Hall and Sobel 2013). For generality, we also include in our analysis tracks that impact the Chesapeake Bay or Delmarva Peninsula after initially crossing the North Carolina coast. Due to the geographic orientation, most TCs that enter the Chesapeake Bay do so by first skirting the North Carolina coastline.

To summarize, a mid-Atlantic TC landfall is considered to take place when: 1) the mid-Atlantic coastline (as defined above) is intersected from the sea by a TC track; or 2) the water-to-land transition occurring along the Chesapeake Bay or Delmarva coastlines is preceded by landfall in the North Carolina. These events could be one of multiple landfalls in a TC life cycle (i.e., we do not consider only the first landfalls). If the same TC makes landfall in the mid-Atlantic as described above more than once only the first occurrence is counted.

d. *Observational data*

To validate model results we use observed TC track data from the International Best Track Archive for Climate Stewardship (IBTrACS; version v03r07; Knapp et al. 2010). This dataset contains TC positions, the 1-min maximum sustained wind (MSW), and the minimum surface pressure estimates for all North Atlantic storms from 1851 to present. For closer correspondence with model definition of MSW (see Manganello et al. 2016), we convert the 1-min MSW to the 10-min average using a conversion coefficient of 0.88 (see Knapp et al. 2010).

Observed mid-Atlantic TC landfalls are then identified using geographic definition in section 2c and, for the direct comparison with model-simulated tracks, by applying lifetime filter of 2 days and the TC identification criteria 1, 4, and 5 in Table 1 (see section 2b). To summarize, the observed TC tracks with landfall in the mid-Atlantic considered in this study occur during the May–November (MJJASON) season, originate south of 30°N, last 2 days or longer and jointly maintain tropical storm equivalent intensity or higher and "tropical in nature" assignment[3] for at least 24 h.

[3] We refer to the "TS" coding used in IBTrACS to report the storm nature or type.

During 1851–2016, only twenty such land-falling events took place (see Fig. 1) with only five during the recent observational period of 1980–2016. These recent TCs are Tropical Storm Dean (1983), Hurricane Bertha (1996), Hurricane Floyd (1999), Hurricane Irene (2011), and Hurricane Sandy (2012). (The corresponding TC tracks simulated in Minerva hindcasts at T1279 and T319 are shown in Figs. S1 and S2, respectively, in the online supplemental material.) We recognize that the operational storm classification is primarily based on the interpretation of satellite observations using empirical methods such as the Dvorak scheme and the Herbert and Poteat technique (Velden et al. 2006), which differs from applying the TC identification criteria in section 2b. Nevertheless, several studies (e.g., Strachan et al. 2013; Murakami 2014; Hodges et al. 2017) have shown that nearly all TCs present in IBTrACS can be successfully identified in different reanalysis datasets by applying similar detection criteria as used here.

For observational estimates of upper-air fields, we use the ECMWF interim reanalysis (ERA-I; Dee et al. 2011) for the period 1980–2012. This data are also prefiltered at T21 (see section 2a).

3. Climatological characteristics of mid-Atlantic tropical cyclone landfalls

The average rate of mid-Atlantic TC landfalls from the observational estimates is 0.10–0.12 yr^{-1} (return period of 8–10 years), which compares quite well with the rate of 0.09–0.10 yr^{-1} (return period of 10–11 years) from the ensemble of Minerva hindcasts (see Table 2). Alternatively, based on the Poisson distribution, which is useful for describing rare extreme events, the probability of one or more TCs making landfall in the mid-Atlantic during the same season is 10%–11% and 9% from the observations and hindcasts, respectively. The differences between these observed and simulated values are not significant at the 95% confidence limit (Table 2). Although the above probabilities are fairly small in a given season, the probabilities of one or more mid-Atlantic TC landfall over 10-yr period are considerable: 66%–72% and 61%–64% based on observations and hindcasts, respectively (Table 2).

There are roughly two regions in the simulations where these land-falling TCs originate: eastern tropical Atlantic and the region off the Southeast U. S. coast (Figs. 2b–d), which shows correspondence with the observed genesis locations (Fig. 2a) and is similar to the observational study of Kocin and Keller (1991). [The shift of the eastern tropical Atlantic center to the east in the simulations is partly a result of the tracking scheme capturing the early (African easterly wave, or AEW) stage of the TC development.] Storms that develop over the eastern tropical Atlantic (e.g., Cape

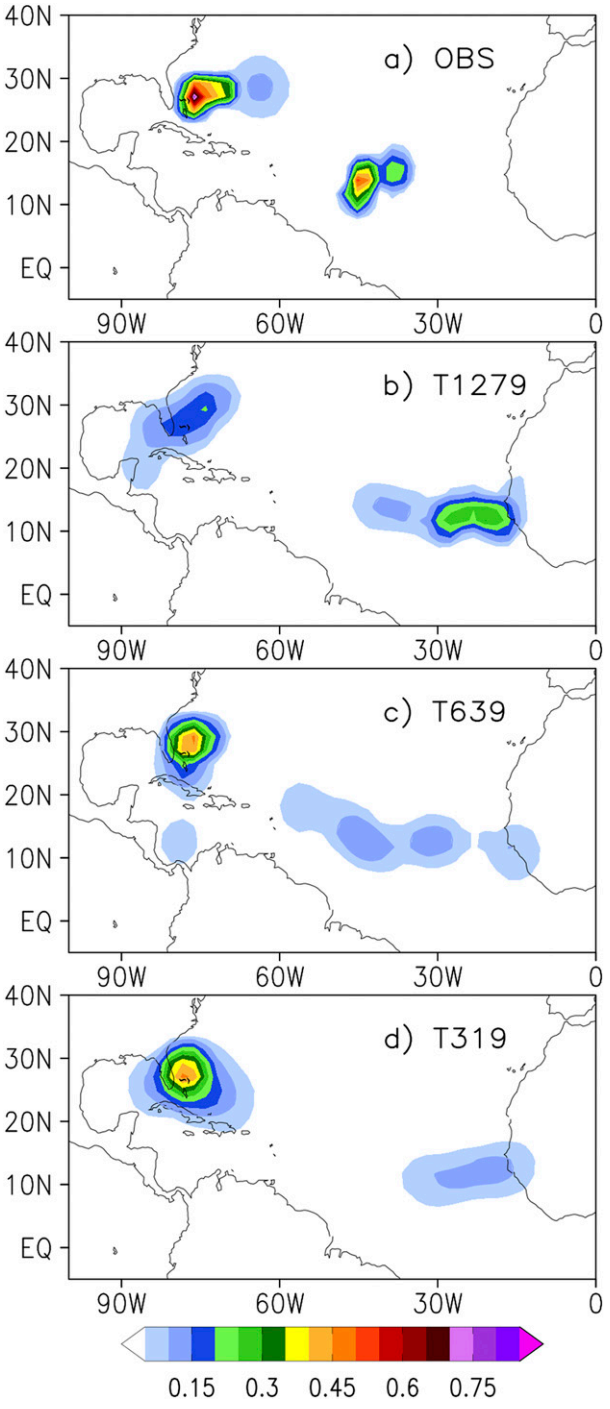

FIG. 2. Genesis densities of TCs with landfalls in the mid-Atlantic as number density per season per unit area equivalent to a 5° spherical cap for (a) IBTrACS data (OBS; 1990–2016) and Minerva hindcasts at (b) T1279, (c) T639, and (d) T319 resolutions.

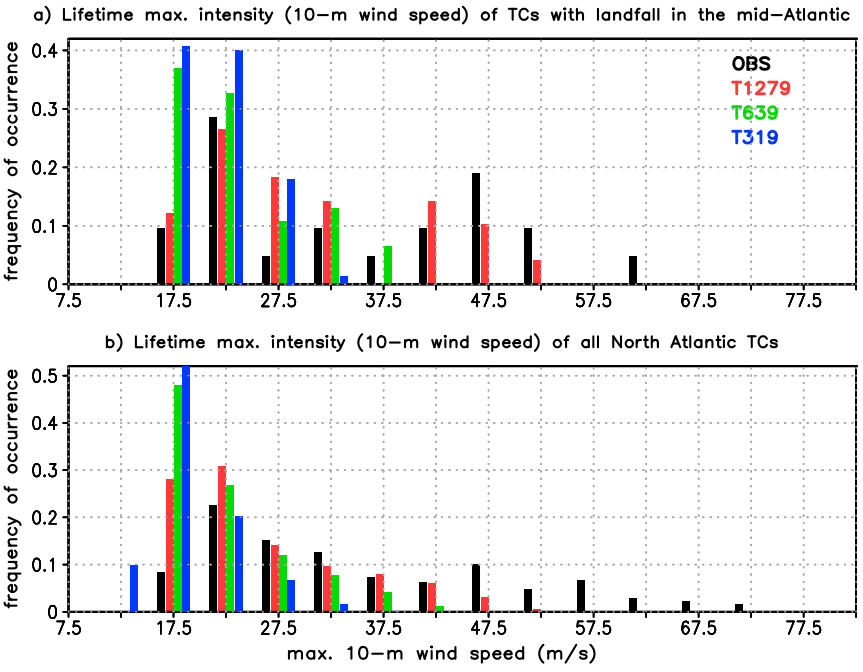

FIG. 3. Distribution of maximum attained 10-m wind speed for (a) TCs with landfall in the mid-Atlantic from IBTrACS data (OBS; 1851–2016) and Minerva hindcasts (1980–2013); and (b) all North Atlantic TCs from IBTrACS data (OBS) and Minerva hindcasts for 1980–2011.

Verde hurricanes) are known to have higher tendency to recurve and reach the East Coast compared to storms that develop farther west (e.g., Elsner et al. 2000; Kossin et al. 2010). It is curious that for the highest-resolution hindcasts (T1279; Fig. 2b), genesis is fairly evenly split between these two main regions (similar to the observed sample of 12 TCs in Fig. 2a) in contrast to T639 and T319 (Figs. 2c,d), even though the overall genesis density distributions (for all North Atlantic TCs) are quite comparable between T1279 and T639 [see Figs. 1b and c in Manganello et al. (2016)]. Comparing T1279 to T319, it is feasible that the increase in genesis in the eastern tropical Atlantic with the model resolution could be related to the improved climatological genesis distribution at higher resolution [cf. Figs. 1b and 1d in Manganello et al. (2016)].

Lifetime maximum intensity of TCs with landfalls in the mid-Atlantic is well simulated only at T1279 (Fig. 3a), where the correspondence to observations at the right tail of distributions appears to be better than for all North Atlantic TCs during 1980–2011 (Fig. 3b). The seasonal cycle of these events is also quite realistic: a clearly defined peak during August–September is captured at T1279 and T639 with less skill at T319 even though the climatological seasonal cycle of all North Atlantic TCs is fairly flat in Minerva (see Fig. 4). The higher frequency of land-falling TCs (and all North Atlantic TCs) in August relative to September at T1279 and T639 is likely due to the earlier identification of the model TCs (i.e., capturing the AEW precursor disturbances) compared to observations.

The above results suggest that Minerva hindcasts exhibit skill in reproducing the climatological characteristics of mid-Atlantic TC landfalls particularly at the highest T1279 resolution.

4. Predictability of mid-Atlantic tropical cyclone landfalls in Minerva

Minerva hindcasts are not skillful in predicting mid-Atlantic TC landfalls on seasonal time scales, although the T1279 model shows a fairly large area of significant skill along the U.S. mid-Atlantic seaboard in TC track predictions [see Fig. 8a in Manganello et al. (2016)]. However, these hindcasts are initialized early in the season (1 May), and there may be potential for skill if initialized later in the season. The assessment is further complicated by the fact that there are only six such observed events during the recent historical (hindcast) period (see section 2d). Nonetheless, encouraged by the results of the previous section the numerical forecasts are further interrogated to identify regional and large-scale environmental conditions associated with these rare TC tracks in order to better quantify their predictability

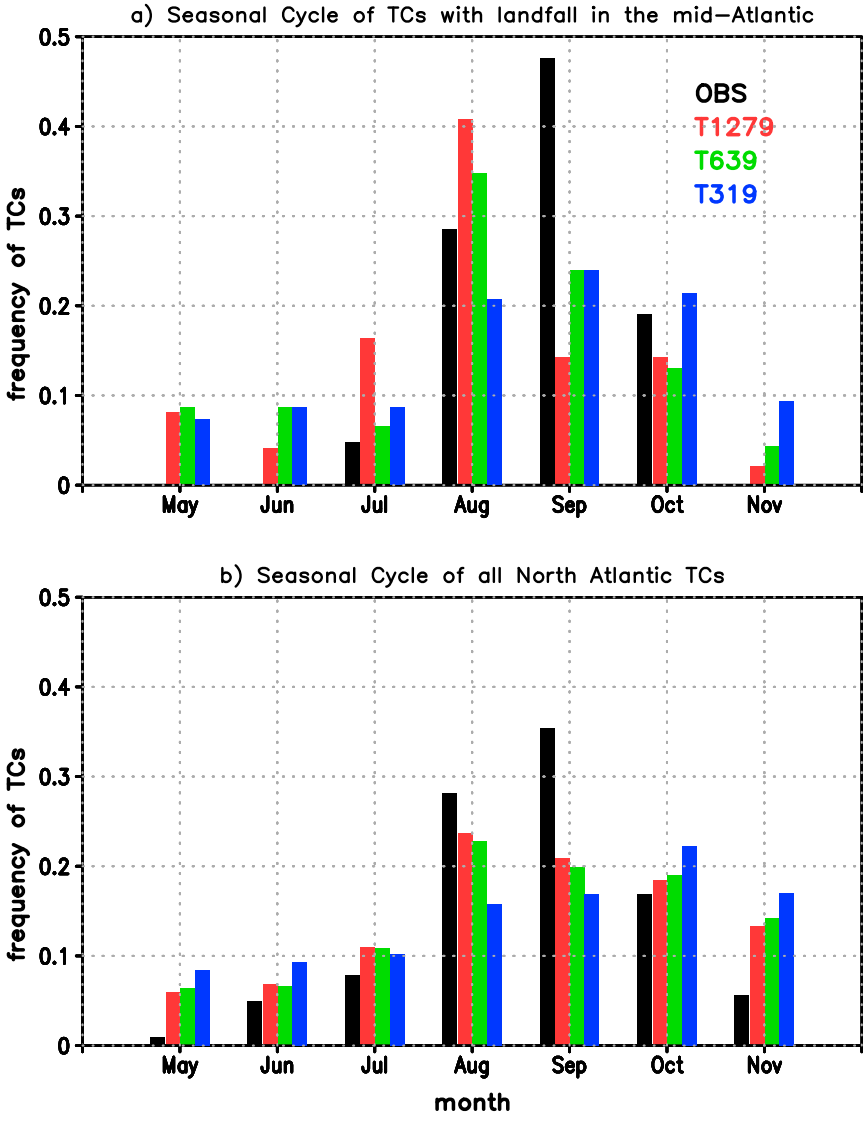

FIG. 4. Seasonal cycle of (a) TCs with landfall in the mid-Atlantic from IBTrACS data (OBS; 1851–2016) and Minerva hindcasts (1980–2013); and (b) all North Atlantic TCs from IBTrACS data (OBS) and Minerva hindcasts for 1980–2011.

on synoptic time scales and its limits, and their dependence on model resolution.

a. Atmospheric conditions during mid-Atlantic TC landfalls

The mean atmospheric circulation anomalies averaged over all mid-Atlantic TC landfalls in Minerva hindcasts at T1279 (49 events; based on daily data) are shown in Fig. 5. (Results are similar for T319.) Based on the pattern of the 700-hPa zonal wind (U700) anomalies, there is an indication of a split in the Atlantic midlatitude jet stream over the western North Atlantic with positive zonal wind anomalies to the north and south of the climatological jet axis and negative anomalies over the northeastern United States (tripole structure; Fig. 5a). This results in very weak westerly (or even weak easterly) winds over the region (not shown), which contribute to steering storms onshore. The flow changes appear to have barotropic structure: similar anomalies are present in the upper troposphere (Fig. 5b). A distinct dipole structure with a blocking anticyclone over the mid-Atlantic is seen in the 500-hPa geopotential height field (Z500; Fig. 5c), which prevents TCs from moving northeastward away from the coast. This is consistent with the occurrence of large-scale cyclonic Rossby wave breaking (Fig. 5d). The above atmospheric conditions are similar to the large-scale flow patterns

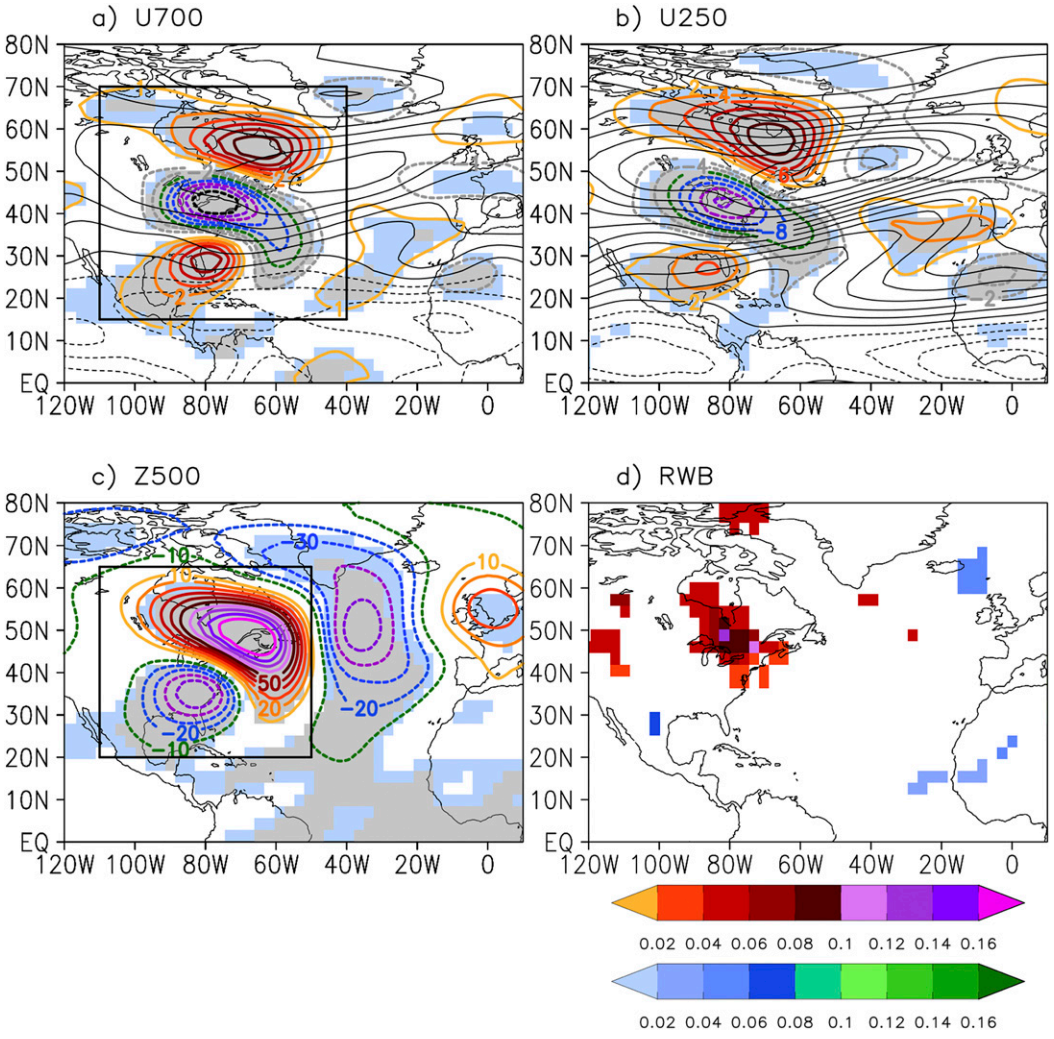

FIG. 5. Composite daily mean (a) 700-hPa (U700) and (b) 250-hPa zonal wind anomalies, (c) 500-hPa geopotential height anomalies (Z500), and (d) frequency of Rossby wave breaking (RWB) averaged over all mid-Atlantic TC landfalls in Minerva hindcasts at T1279. Contour intervals are 1 m s^{-1} in (a), 2 m s^{-1} in (b), and 10 m in (c). Negative contours are dashed, zero contour is omitted. Blue (gray) shading shows statistical significance at the 95% (99%) confidence level using Monte Carlo simulation. Black contours in (a) and (b) denote July–October climatological zonal winds with the contour interval of 2 m s^{-1}. In (d), only the values statistically significant at the 90% confidence levels using Monte Carlo simulation are shown; cyclonic (anticyclonic) RWB frequency is depicted by red/purple (blue/green) colors, and it represents a fractional probability of occurrence. Note that RWB is detected as the large-scale overturning (north–south gradient reversal) of 250-hPa absolute vorticity. U700 tripole and Z500 dipole patterns are designated by black boxes in (a) and (c), respectively.

that occurred during Hurricane Sandy (e.g., Fig. 1 in Barnes et al. 2013).

A question arises of how frequent (or common) are the occurrences of the Z500 dipole and the U700 tripole patterns discussed above at the time of mid-Atlantic TC landfalls in Minerva. Frequency distributions in Fig. 6 demonstrate that about 82%–86% (71%–80%) of all mid-Atlantic TC landfalls are associated with the anomalous Z500 dipole (U700 tripole) pattern. Moreover, all other TCs that are within the proximity of the U.S. East Coast (within approximately the same distance where the land-falling TCs are located 1 day prior to the landfall; see the region outlined in thick dashed in Fig. 12), but do not make mid-Atlantic landfall, are rarely associated with this pattern, and the results of Monte Carlo simulation drawn from this sample are largely similar to the climatological distribution (not shown). It is also noteworthy that the anomalous atmospheric conditions like the ones shown in Figs. 5a and 5c are not so common both in the simulations

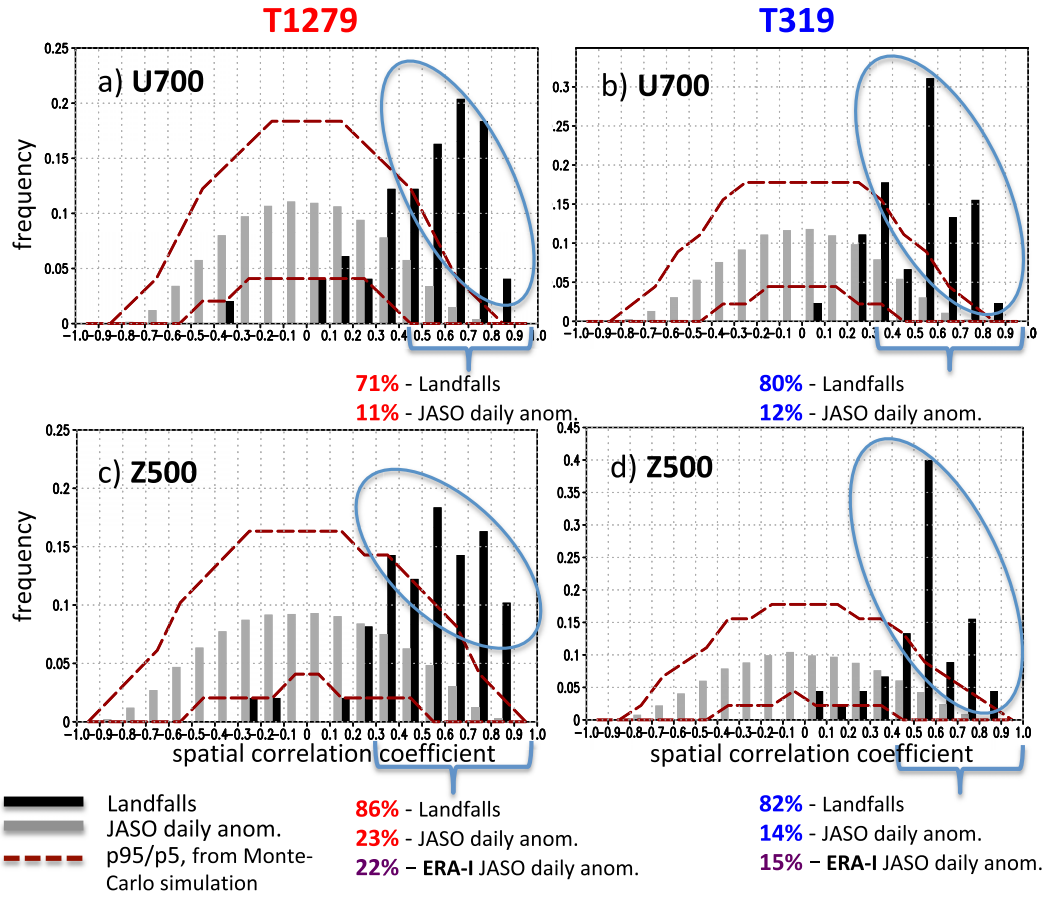

FIG. 6. Frequency distributions of spatial correlation coefficient (scorr) between the (a),(b) daily 700-hPa zonal wind anomalies and the tripole pattern (within black box area in Fig. 5a); and between the (c),(d) daily 500-hPa geopotential height anomalies and the dipole pattern (within black box area in Fig. 5c) for mid-Atlantic TC landfall events (black bars) and all July–October (JASO) daily anomalies (gray bars) for (left) T1279 and (right) T319. Dashed brown lines show the 5th and 95th percentiles from Monte-Carlo simulation. Numbers under the figures show the percent of landfalling events with the statistically significant scorr values based on Monte Carlo simulations and the corresponding cumulative frequency for JASO climatology, for Minerva (red and blue), and ERA-I (purple).

and the reanalysis: the cumulative frequency of occurrence ranges between 15% and 22% (11%–12%) for Z500 (U700; see Fig. 6).

b. *Persistence of local finite-amplitude wave activity anomalies leading to mid-Atlantic TC landfalls*

The evolution of the atmospheric flow patterns leading to mid-Atlantic TC landfalls is further analyzed using local finite-amplitude wave activity (LWA; Huang and Nakamura 2016; see Fig. 1 in Chen et al. 2015). LWA has been shown to be an effective diagnostic of localized weather extremes, such as atmospheric blocking where a close correspondence between large LWA events and the reversal of zonal wind has been noted (Chen et al. 2015; Huang and Nakamura 2016). Specifically, local wave amplification associated with the pronounced blocking episode that steered Hurricane Sandy to the U.S. East Coast is well captured by a large-amplitude quasi-stationary LWA (Huang and Nakamura 2016). We apply the LWA diagnostic to daily mean Z500. By construction, the computed LWA and its southern and northern components have positive values. The northern (southern) LWA emphasizes the northward (southward) displacement in height, or blocking high (synoptic low) conditions, and the corresponding anticyclonic (cyclonic) wave breaking (not shown). A more detailed description of the LWA calculation can also be found in Swenson et al. (2018). Composite LWA anomalies at landfall corresponding to the Z500 anomalies in Fig. 5c are shown in Fig. 7. The Z500 dipole structure is clearly identified as a large-amplitude positive LWA anomaly extending southeastward to the tropical latitudes flanked by negative LWA anomalies to the northeast and the southwest (Fig. 7a). There is

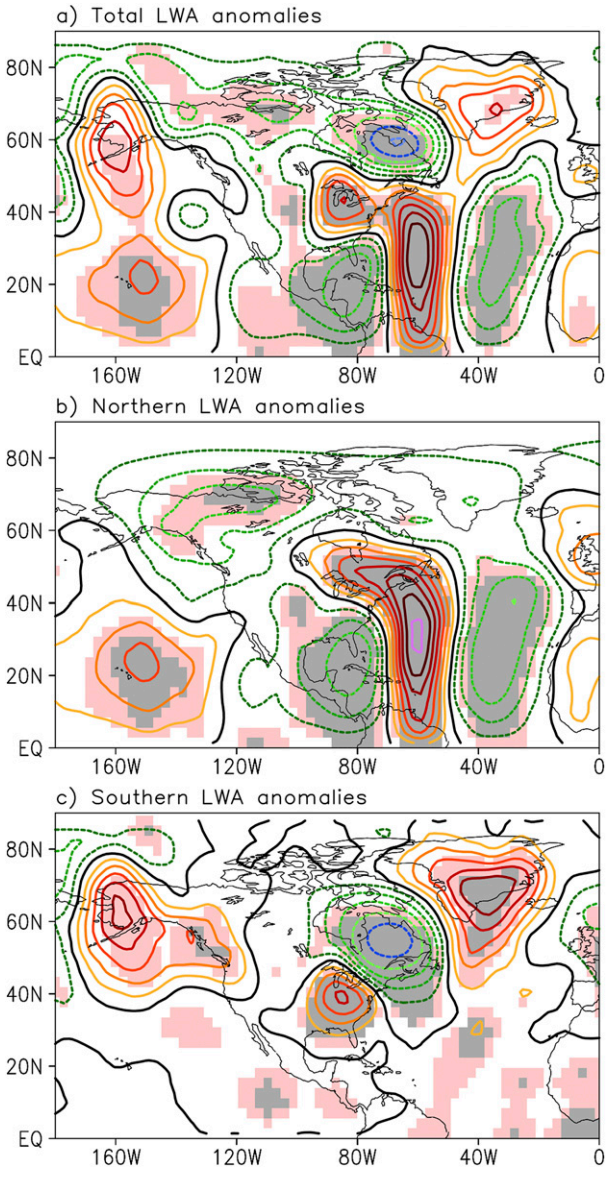

FIG. 7. Composite daily mean (a) total, (b) northern, and (c) southern LWA anomalies averaged over all mid-Atlantic TC landfalls in Minerva hindcasts at T1279. Contour interval is 0.5×10^8 m^2. Negative contours are green/blue and dashed, positive contours are red/yellow and solid, zero contour is black. Pink (gray) shading shows statistical significance at the 95% (99%) confidence level using Monte Carlo simulation.

consequently a close correspondence between this LWA pattern and zonal wind changes in Figs. 5a and 5b where positive (negative) LWA anomalies are collocated with the weakened (strengthened) jet. This anomalous LWA pattern is largely due to a strongly enhanced northern LWA in the region and a weakened southern (northern) LWA to the northeast (southwest; Figs. 7b,c). Over the western North Atlantic, these results are similar to T319 (not shown).

Large LWA events are often characterized by the long buildup and persistence of the anomalies. Figure 8 shows the evolution of the composite northern and southern LWA anomalies for T1279 starting at 4 days prior to landfall. There exist large-amplitude quasi-stationary features in the LWA anomaly distribution over the Gulf of Mexico and western Caribbean (Reg1 hereafter; see boxed areas in Figs. 8a–e), western North Atlantic (Reg2; see boxed areas in Figs. 8f–j) and eastern North Pacific (Reg3; Figs. 8a–e) that persist up to 4 days leading to these land-falling events. (Reg1 exhibits statistically significant anomalies as early as at 5- and 6-day leads—not shown). Curiously, strongly enhanced northern LWA over the North Atlantic does not show strong persistence: this central feature appears to originate only at 2-day lead off the U.S. East Coast (Fig. 8c). While again results for T319 are overall similar to T1279, there is one notable difference: the northern LWA anomalies over Reg3 are largely insignificant at all leads (not shown).

To further quantify predictability of landfalls associated with the large anomalous LWA patterns described above, we introduce an LWA index (LWAI hereafter) by averaging northern and southern LWA anomalies over the selected regions as specified above and several days prior to landfall:

$$\mathrm{LWAI} = -1 \times (\mathrm{NLWA1} + \mathrm{SLWA2} + \mathrm{NLWA3}), \quad (1)$$

where NLWA1 denotes northern LWA anomalies averaged over Reg1, SLWA2 is southern LWA anomalies averaged over Reg2, and NLWA3 is northern LWA anomalies averaged over Reg3. We have found that 3-day temporal averaging is most beneficial and we consider LWAI at 1-day and 2-day lead (LWAI1-day and LWAI2-day hereafter) corresponding to the LWAI averaged over 1–3 days and 2–4 days prior to landfall, respectively. Frequency distributions of the LWAI1-day and LWAI2-day demonstrate a statistically significant shift with respect to July–October daily anomalies at T1279, whereas results for T319 are largely insignificant (not shown). This suggests a potential for the LWAI to serve as a predictor of mid-Atlantic TC landfalls at 1- and 2-day leads mainly for the T1279 model. This potential is further evaluated in section 5 where a statistical model to predict mid-Atlantic TC landfalls based on the LWAI as a predictor is developed and assessed.

c. *Oceanic conditions during mid-Atlantic TC landfalls*

In a coupled forecasting system, predictability also stems from the ocean which has longer memory

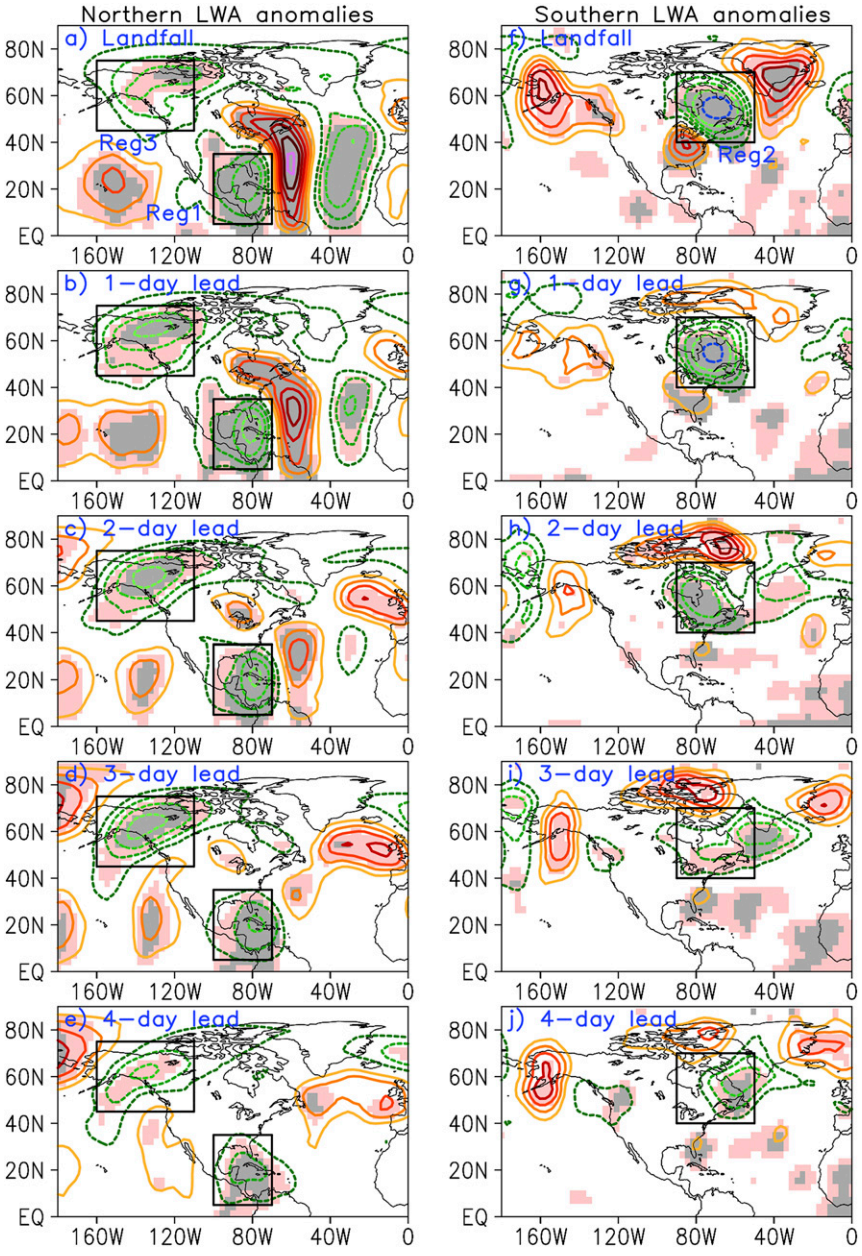

FIG. 8. Composite daily mean (left) northern and (right) southern LWA anomalies averaged over all mid-Atlantic TC landfalls in Minerva hindcasts at T1279 at different leads prior to landfall. Contour interval is 0.5×10^8 m^2. Negative contours are green/blue and dashed, positive contours are red/yellow and solid, zero contour is omitted. Pink (gray) shading shows statistical significance at the 95% (99%) confidence level using Monte Carlo simulation. Black rectangles show the regions where LWA anomalies are averaged to construct the LWA index.

compared to the atmosphere. We therefore examine here whether mid-Atlantic TC landfalls in Minerva are associated with persistent sea surface temperature (SST) anomalies. Figure 9 shows composite detrended SST anomalies (SSTAs) at selected leads prior to landfalls at T1279. Large-scale SSTAs off the U.S. East Coast at the time of landfall (Fig. 9a) are likely forced by surface wind anomalies related to the split in the midlatitude jet stream (Fig. 5a; see section 4a): negative zonal wind anomalies over the northeast U.S. and positive ones to the south are roughly collocated with positive and negative SSTAs, respectively. This SST response fades away at longer leads consistent with the atmospheric flow changes in Fig. 8. On the

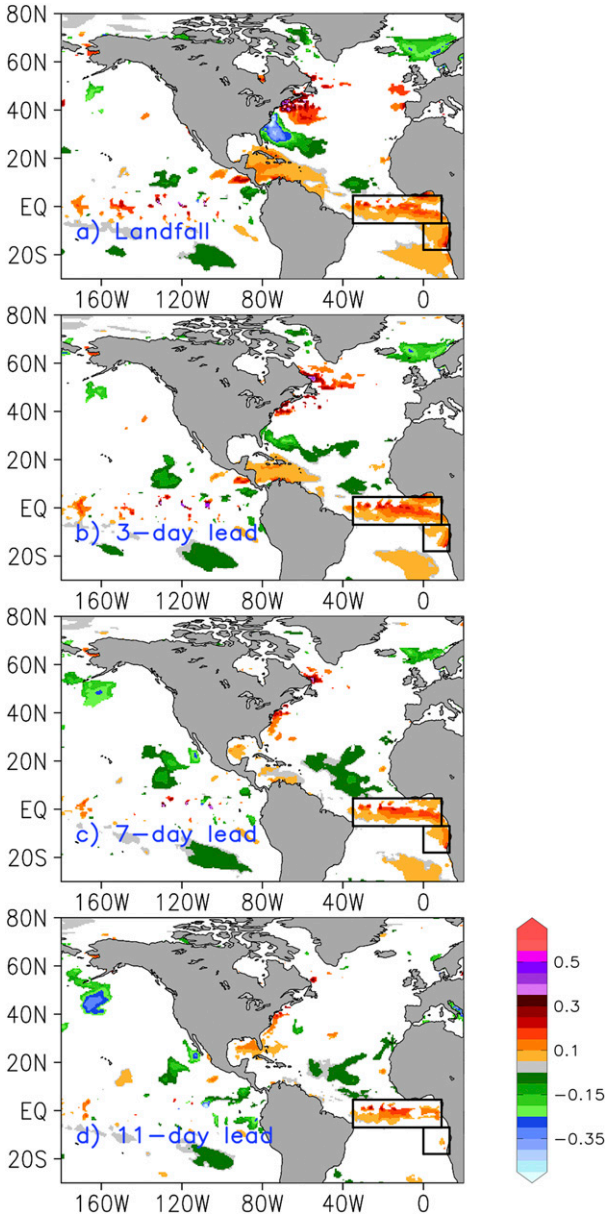

FIG. 9. Composite daily mean SST anomalies averaged over all mid-Atlantic TC landfalls in Minerva hindcasts at T1279 at (a) landfall, and (b) 3-day, (c) 7-day, and (d) 11-day lead prior to landfall. Units are °C. Only values that are statistically significant at the 95% confidence level using Monte Carlo simulation are shown. Black rectangles denote the regions where SST anomalies are averaged to construct the SST index.

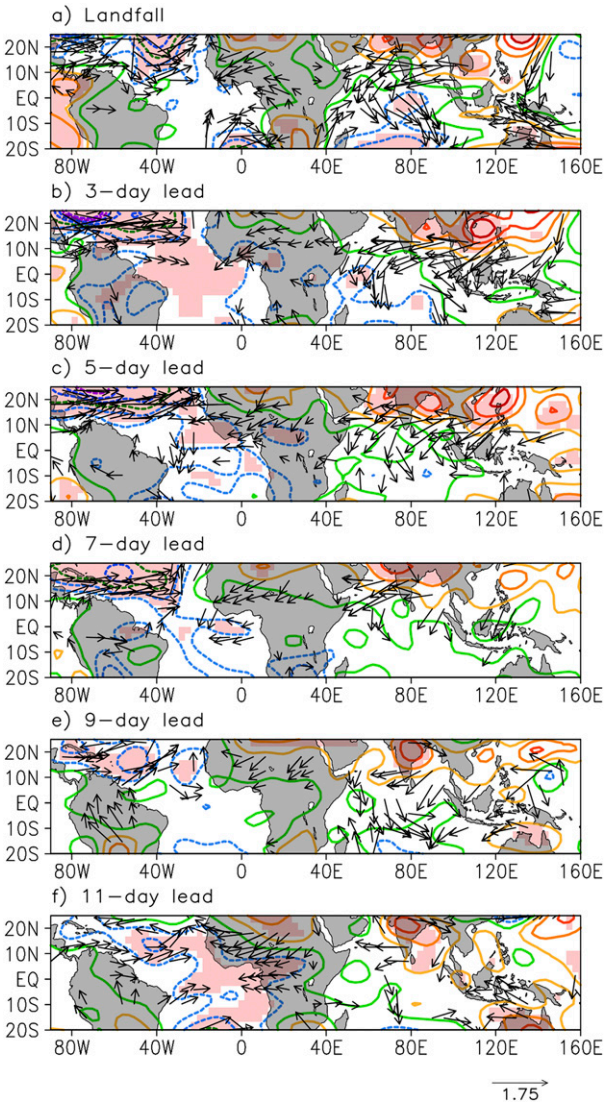

FIG. 10. Composite daily mean 925-hPa wind and geopotential height anomalies averaged over all mid-Atlantic TC landfalls in Minerva hindcasts at T1279 at different leads prior to landfall. The arrow is 1.75 m s^{-1} representing the unit vector of 925-hPa wind in the panels. Vector arrows are plotted only when either of the wind components is statistically significant at the 95% confidence level using Monte Carlo simulation. Contour interval is 2 m. Negative contours are blue/purple and dashed, positive contours are red/yellow and solid, zero contour is bright green. Pink shading shows statistical significance of the 925-hPa geopotential height anomalies at the 95% confidence level.

other hand, in the vicinity of the equatorial Atlantic, the SSTAs persist for about 2 weeks preceding TC landfalls. To shed some light on the origin of these equatorial SSTAs, Fig. 10 shows composite lower-tropospheric wind and geopotential height anomalies at selected leads prior to landfalls. 925-hPa wind exhibits significant large-scale westerly anomalies over the tropical North Atlantic that weaken somewhat at 9-day and longer leads. These changes are collocated with significant negative 925-hPa geopotential height anomalies extending at some leads to the equatorial Atlantic and tropical South Atlantic. Positive equatorial SSTAs in Fig. 9 are consistent with these anomalous surface westerlies (Fig. 10), which would reduce the strength of

the mean easterly trade winds and turbulent fluxes from the ocean. It is curious that the atmospheric flow changes over the tropical Atlantic are accompanied by coherent anomalous northeasterlies over the north Indian Ocean crossing the equator and changing to northwesterlies (Fig. 10). The concurrent positive 925-hPa geopotential height anomalies over South Asia along with the corresponding wind changes are indicative of the reduction in the strength of the Asian monsoon.

To relate equatorial SSTAs to the occurrence of the mid-Atlantic TC landfalls, we examine vertical wind shear(VWS) anomalies as the near-surface wind changes discussed above would have a direct impact on this large-scale parameter known to influence tropical cyclogenesis and intensification. Figure 11 shows composite 200–925-hPa zonal VWS anomalies (Ventrice et al. 2011) at all leads between 9 days and landfall. The reduction in VWS as evidenced by anomalous easterly shear over the main development region (MDR; 7.5°–22.5°N, 80°–20°W) is present at all leads shown. This reduction in VWS along with the reduced lower-tropospheric geopotential height would favor the formation and development of the land-falling TCs that originate in the eastern tropical Atlantic.

Similar to the LWAI, an SST index (SSTI) is constructed by averaging SST anomalies over the equatorial Atlantic region marked by black rectangles in Fig. 9. The ability of the SSTI to serve as a predictor of mid-Atlantic TC landfalls on synoptic time scales is evaluated in section 5. Curiously, no significant SST anomalies at longer than 2-day leads prior to mid-Atlantic TC landfalls are found in the T319 hindcasts.

5. Binary quantile regression model of mid-Atlantic tropical cyclone landfalls in Minerva

Here we evaluate the ability of the LWAI and SSTI to serve as predictors of mid-Atlantic TC landfalls on synoptic time scales using a statistical model, and results presented in sections 4b and 4c. To form a representative data sample, we consider all other simulated TC positions (daily) during the July–October season that fall approximately within a similar distance from the coast as land-falling TCs are at 1- or 2-day lead (see the regions outlined in thick dashed and solid, respectively, in Fig. 12). These other TC positions are used in the statistical model as ''No Landfall'', or ''Zero'' events, as opposed to ''Landfall'', or ''One'' events. LWAI and SSTI are computed for ''No Landfall'' events in the same manner as described above. Naturally, for the mid-Atlantic coastline, there are a lot more ''No Landfall'' than ''Landfall'' events. In fact, landfalls correspond to only 1.5%–1.9% (1-day lead) and 0.7%–0.9% (2-day lead) of all data in the sample. This type of data, which consists of binary dependent variables with dozens to thousands of times fewer ones (events) than zeros (nonevents) belongs to the category of *rare events* data according to King and Zeng (2001). This is also a case of *unbalanced* data (relative rareness) (i.e., when the minority class or class of interest is much smaller than the majority class). Classification algorithms generally suffer when data are skewed toward one class (Van der Paal 2014).

We choose binary quantile regression as a statistical model since it uses skewed link functions (higher quantiles) which are found to offer a better fit to unbalanced data (Kordas 2006; Van der Paal 2014). Selecting a high quantile places more weight on the rare event, and centers estimation around the informative part of the sample. We use the function *rq.bin* in package *Qtools* for R (Geraci 2016, 2018) to estimate the binary quantile regression model where the LWAI, SSTI, and both LWAI and SSTI[4] are tested as predictors:

$$g_\tau[P(y=1)] \sim \text{LWAI}, \tag{2}$$

$$g_\tau[P(y=1)] \sim \text{SSTI}, \tag{3}$$

$$g_\tau[P(y=1)] \sim \text{LWAI} + \text{SSTI}, \tag{4}$$

where g_τ [ ] is the τ quantile link function derived from the sample, and $\tau = 1 - \overline{y}$, where $\overline{y}$ is the overall sample probability P (y = 1).

The K-fold cross validation is performed on the model where the dataset is split in K partitions, of which $K - 1$ are used for training (building the model) and the remaining partition for testing (generating predictions). The dataset is split in random divisions, each containing an equal number of ''Landfall'' events. We use K values of 7 and 5 for T1279 and T319, respectively. The cross-validation procedure is repeated K times, with each of the K partitions used exactly once as the validation data until predictions are obtained for the whole sample. The predictive performance of the model is assessed using the area under the receiver operating characteristic (ROC) curve, or AUC, as a skill metric since it is not sensitive to class imbalance. Using the LWAI as a predictor, the statistical model shows moderate skill in predicting mid-Atlantic TC landfalls at 1-day lead with somewhat lower skill at 2-day lead and marginal skill scores for T319 (Table 3). The SSTI has lower predictive value compared to the LWAI, and the addition of the

[4] The LWAI and SSTI are found to be uncorrelated.

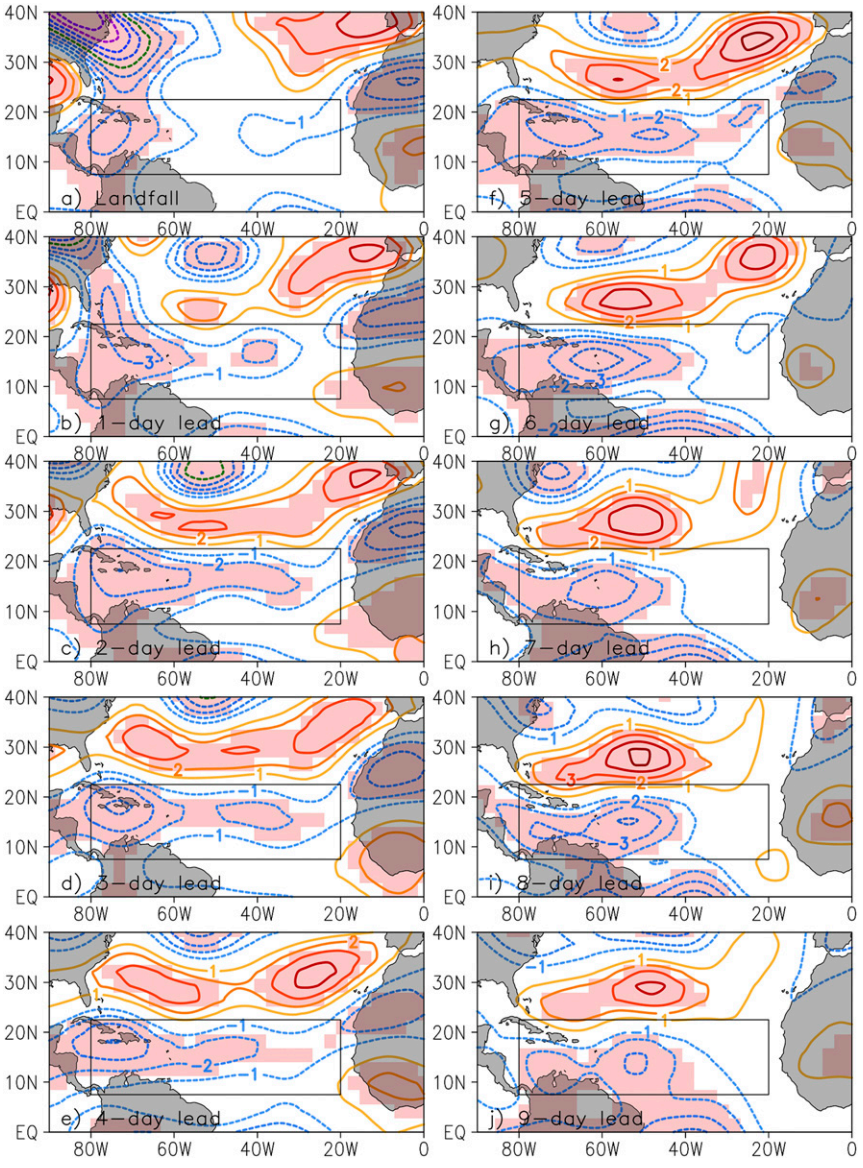

FIG. 11. Composite daily mean 200–925-hPa vertical wind shear anomalies of the zonal wind averaged over all mid-Atlantic TC landfalls in Minerva hindcasts at T1279 at all leads between 9 days and landfall. Contour interval is 1 m s^{-1}. Negative contours are blue/purple and dashed, positive contours are red/yellow and solid, zero contour is omitted. Pink shading shows statistical significance at the 95% confidence level using Monte Carlo simulation. Black rectangles delineate the main development region (MDR; 7.5°–22.5°N, 80°–20°W).

SSTI to the model does not improve the skill scores substantially. Although these results may be of limited use to the operational forecasting, we see a potential benefit of our analysis to longer time-scale predictions (see further discussion below).

6. Summary and conclusions

Multimodel ensemble seasonal hindcasts with a high-atmospheric-resolution coupled prediction system based on the ECMWF System 4 (Project Minerva) have been used to study predictability of the mid-Atlantic TC landfalls, which are among the most infrequent landfalls along the U.S. East Coast. We have verified that Minerva historical forecasts exhibit skill in simulating basic statistics and climatological characteristics of these landfalling TCs where many features are reproduced with higher fidelity at the highest atmospheric horizontal spectral resolution of T1279 (16-km grid spacing). Because model resolution for the most part is not sufficiently

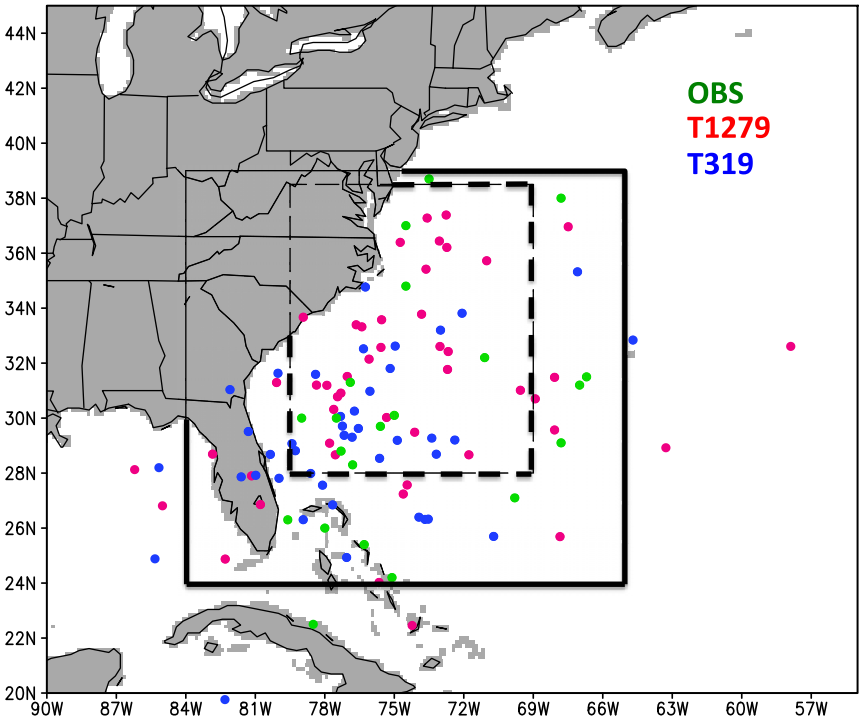

FIG. 12. Positions of TCs (dots) with landfall over the mid-Atlantic region 2 days prior to landfall in IBTrACS (OBS; green), and Minerva hindcasts at T1279 (red) and T319 (blue). Outlined regions in thick solid (dashed) denote geographic areas encompassing all other TC positions used in the statistical model as "No Landfall", or "Zero" events, at 2-day (1-day) lead.

high to represent the intense hurricanes realistically, we focus exclusively on tracks and do not examine intensity at landfall nor distinguish between intensity classes in this study.

A vast majority of TC tracks with landfalls in the mid-Atlantic in Minerva are associated with specific anomalous atmospheric conditions (Z500 dipole and U700 tripole patterns, large-scale cyclonic Rossby wave breaking), which are quite similar to the weather patterns that occurred during Hurricane Sandy's landfall and are overall fairly infrequent in the simulations and the reanalysis. When the evolution of these atmospheric flow patterns is investigated using LWA, an effective diagnostic of weather extremes at the regional scales, we are able to identify large-amplitude quasi-stationary features in the composite LWA anomaly distribution that persist up to about a week leading to these land-falling events. An LWA index formed by geographic and temporal averaging of the LWA anomalies over the regions of high persistence demonstrates a potential to serve as a predictor of mid-Atlantic TC landfalls at 1- and 2-day leads mainly for the T1279 model. In this model, we also find significant SST anomalies in the equatorial Atlantic that persist for about 2 weeks leading to mid-Atlantic TC landfalls and are likely an ocean response to the anomalous surface westerlies over the tropical North Atlantic.

To test the predictive capability of the LWA and SST indices, we have developed a binary quantile regression model of mid-Atlantic TC landfalls in Minerva using these indices individually and in combination as predictors. With the LWA index as a predictor, the statistical model shows moderate skill at 1-day and 2-day

TABLE 3. Area under the receiver operating characteristic (ROC) curve (AUC) for binary quantile regression models with the LWAI, SSTI, and LWAI + SSTI as predictors of mid-Atlantic TC landfalls in T1279 and T319. The K-fold cross validation is used on the regression models (see section 5). SSTI is not used for T319 based on the results in section 4c.

	$g_\tau [P(y=1)] \sim$ LWAI	$g_\tau [P(y=1)] \sim$ SSTI	$g_\tau [P(y=1)] \sim$ LWAI + SSTI
		1-day lead	
T1279	0.66	0.61	0.68
T319	0.59	—	—
		2-day lead	
T1279	0.63	0.60	0.63
T319	0.58	—	—

leads at T1279 and marginal skill scores for T319. The SST index has lower predictive value compared to the LWA index, and its addition to the model does not lead to marked improvement of the skill scores.

With respect to these results a few important questions remain that will be the subject of future work:

1) What is the nature of the persistent LWA anomalies? Are they forced or part of the natural variability of atmospheric circulation?
2) Is there a value in the LWA index as a predictor of mid-Atlantic TC landfalls on decadal and longer time scales?
3) Why are there differences between the T1279 and T319 models with respect to the geographical location of the persistent LWA anomalies? And why are there no persistent SST anomalies in the T319 model, which has the same ocean resolution as the T1279 model?

The results of this study may be of limited value to the operational forecasting. For example, the landfall location of Hurricane Sandy has been predicted quite accurately at 5-day to 7-day lead times (e.g., Kerr 2012; Xiang et al. 2015), although the westward bend of TC tracks like Sandy's continue to pose a great forecasting challenge. Instead, we see a potential benefit of our analysis to longer time-scale predictions (e.g., decadal) including climate change projections where the bulk of models used are of coarse resolution and therefore may not faithfully reproduce the statistics of land-falling TCs and/or it is computationally prohibitive to perform an explicit TC identification and tracking. In these cases, a change in the LWA index distribution could serve as a proxy for a change in mid-Atlantic TC landfall statistics from one decade to another, or from a cooler to a warmer climate.

Acknowledgments. Funding of COLA for this study is provided by grants from NSF (AGS-1338427), NOAA (NA14OAR4310160), and NASA (NNX14AM19G). Special thanks to the European Centre for Medium-Range Weather Forecasts, particularly Franco Molteni and Frederic Vitart, for designing, planning, and conducting some of the simulations as part of the Minerva project. Computing resources on the Yellowstone supercomputer provided by the National Center for Atmospheric Research are also gratefully acknowledged.

REFERENCES

Barnes, E. A., L. M. Polvani, and A. H. Sobel, 2013: Model projections of atmospheric steering of Sandy-like superstorms. *Proc. Natl. Acad. Sci. USA*, **110**, 15 211–15 215, https://doi.org/10.1073/pnas.1308732110.

Blake, E. S., T. B. Kimberlain, R. G. Berg, J. P. Cangialosi, and J. L. Beven II, 2013: Tropical Cyclone Report, Hurricane Sandy (22–29 October 2012). NHC Tech. Rep. AL182012, National Hurricane Center, 157 pp., https://www.nhc.noaa.gov/data/tcr/AL182012_Sandy.pdf.

Camp, J., M. Roberts, C. MacLachlan, E. Wallace, L. Hermanson, A. Brookshaw, and A. Arribas, and A. A. Scaife, 2015: Seasonal forecasting of tropical storms using the Met Office GloSea5 seasonal forecast system. *Quart. J. Roy. Meteor. Soc.*, **141**, 2206–2219, https://doi.org/10.1002/qj.2516

Cash, B. A., and Coauthors, 2017: Sampling variability and the changing ENSO–monsoon relationship. *Climate Dyn.*, **48**, 4071–4079, https://doi.org/10.1007/S00382-016-3320-3.

Chen, G., J. Lu, D. A. Burrows, and L. R. Leung, 2015: Local finite-amplitude wave activity as an objective diagnostic of midlatitude extreme weather. *Geophys. Res. Lett.*, **42**, 10 952–10 960, https://doi.org/10.1002/2015GL066959.

Dee, D. P., and Coauthors, 2011: The ERA-Interim reanalysis: Configuration and performance of the data assimilation system. *Quart. J. Roy. Meteor. Soc.*, **137**, 553–597, https://doi.org/10.1002/qj.828.

Elsner, J. B., K.-B. Liu, and B. Kocher, 2000: Spatial variations in major U.S. hurricane activity: Statistics and a physical mechanism. *J. Climate*, **13**, 2293–2305, https://doi.org/10.1175/1520-0442(2000)013<2293:SVIMUS>2.0.CO;2.

Emanuel, K., S. Ravela, E. Vivant, and C. Risi, 2006: A statistical deterministic approach to hurricane risk assessment. *Bull. Amer. Meteor. Soc.*, **87**, 299–314, https://doi.org/10.1175/BAMS-87-3-299.

——, R. Sundararajan, and J. Williams, 2008: Hurricanes and global warming: Results from downscaling IPCC AR4 simulations. *Bull. Amer. Meteor. Soc.*, **89**, 347–367, https://doi.org/10.1175/BAMS-89-3-347.

European Centre for Medium-Range Weather Forecasts, 2013: IFS documentation—CY38r1. ECMWF, accessed 12 September 2018, https://www.ecmwf.int/en/forecasts/documentation-and-support/changes-ecmwf-model/ifs-documentation.

Fogarty, C. T., and E. S. Blake, 2013: The double life of Hurricane Sandy—and a climatological perspective of these post-tropical giants [in "State of the Climate in 2012"]. *Bull. Amer. Meteor. Soc.*, **94** (8), S109–S110.

Geraci, M., 2016: Qtools: A collection of models and tools for quantile inference. *R J.*, **8**, 117–138, https://doi.org/10.32614/RJ-2016-037.

——, 2018: Qtools: Utilities for quantiles. R package version 1.3, accessed 15 November 2017, https://cran.r-project.org/package=Qtools.

Hall, T. M., and S. Jewson, 2007: Statistical modeling of North Atlantic tropical cyclone tracks. *Tellus*, **59A**, 486–498, https://doi.org/10.1111/j.1600-0870.2007.00240.x.

——, and A. H. Sobel, 2013: On the impact angle of Hurricane Sandy's New Jersey landfall. *Geophys. Res. Lett.*, **40**, 2312–2315, https://doi.org/10.1002/grl.50395.

——, and E. Yonekura, 2013: North American tropical cyclone landfall and SST: A statistical model study. *J. Climate*, **26**, 8422–8439, https://doi.org/10.1175/JCLI-D-12-00756.1.

Hodges, K. I., 1994: A general method for tracking analysis and its application to meteorological data. *Mon. Wea. Rev.*, **122**, 2573–2586, https://doi.org/10.1175/1520-0493(1994)122<2573:AGMFTA>2.0.CO;2.

——, 1995: Feature tracking on the unit sphere. *Mon. Wea. Rev.*, **123**, 3458–3465, https://doi.org/10.1175/1520-0493(1995)123<3458:FTOTUS>2.0.CO;2.

——, 1999: Adaptive constraints for feature tracking. *Mon. Wea. Rev.*, **127**, 1362–1373, https://doi.org/10.1175/1520-0493(1999)127<1362:ACFFT>2.0.CO;2.

——, A. Cobb, and P. L. Vidale, 2017: How well are tropical cyclones represented in reanalysis datasets? *J. Climate*, **30**, 5243–5264, https://doi.org/10.1175/JCLI-D-16-0557.1.

Huang, C. S. Y., and N. Nakamura, 2016: Local finite-amplitude wave activity as a diagnostic of anomalous weather events. *J. Atmos. Sci.*, **73**, 211–229, https://doi.org/10.1175/JAS-D-15-0194.1.

Kerr, R. A., 2012: One Sandy forecast a bigger winner than others. *Science*, **338**, 736–737, https://doi.org/10.1126/science.338.6108.736.

King, G., and L. Zeng, 2001: Logistic regression in rare events data. *Polit. Anal.*, **9**, 137–163, https://doi.org/10.1093/oxfordjournals.pan.a004868.

Knapp, K. R., M. C. Kruk, D. H. Levinson, H. J. Diamond, and C. J. Neumann, 2010: The International Best Track Archive for Climate Stewardship (IBTrACS). *Bull. Amer. Meteor. Soc.*, **91**, 363–376, https://doi.org/10.1175/2009BAMS2755.1.

Kocin, P. J., and J. H. Keller, 1991: A 100-year climatology of tropical cyclones for the northeast United States. Preprints, *19th Conf. on Hurricanes and Tropical Meteorology*, Miami, FL, Amer. Meteor. Soc., 152–157.

Kordas, G., 2006: Smoothed binary regression quantiles. *J. Appl. Econ.*, **21**, 387–407, https://doi.org/10.1002/jae.843.

Kossin, J. P., S. J. Camargo, and M. Sitkowski, 2010: Climate modulation of North Atlantic hurricane tracks. *J. Climate*, **23**, 3057–3076, https://doi.org/10.1175/2010JCLI3497.1.

Lackmann, G. M., 2015: Hurricane Sandy before and after 2100. *Bull. Amer. Meteor. Soc.*, **96**, 547–560, https://doi.org/10.1175/BAMS-D-14-00123.1.

Landsea, C. W., and Coauthors, 2004: The Atlantic hurricane database reanalysis project: Documentation for the 1851-1910 alterations and additions to the HURDAT database. *Hurricanes and Typhoons: Past, Present and Future*, R. J. Murname and K.-B. Liu, Eds., Columbia University Press, 177–221.

Lau, W. K. M., J. J. Shi, W. K. Tao, and K. M. Kim, 2016: What would happen to Superstorm Sandy under the influence of a substantially warmer Atlantic Ocean? *Geophys. Res. Lett.*, **43**, 802–811, https://doi.org/10.1002/2015GL067050.

Lin, N., K. Emanuel, M. Oppenheimer, and E. Vanmarcke, 2012: Physically based assessment of hurricane surge threat under climate change. *Nat. Climate Change*, **2**, 462–467, https://doi.org/10.1038/nclimate1389.

——, R. E. Kopp, B. P. Horton, and J. P. Donnelly, 2016: Hurricane Sandy's flood frequency increasing from year 1800 to 2100. *Proc. Natl. Acad. Sci. USA*, **113**, 12 071–12 075, https://doi.org/10.1073/pnas.1604386113.

Madec, G., 2008: NEMO ocean engine. Note du Pole de modélisation, Institut Pierre-Simon Laplace (IPSL), Tech. Rep. 27, 396 pp., https://www.nemo-ocean.eu/wp-content/uploads/NEMO_book.pdf.

Manganello, J. V., and Coauthors, 2014: Future changes in the western North Pacific tropical cyclone activity projected by a multidecadal simulation with a 16-km global atmospheric GCM. *J. Climate*, **27**, 7622–7646, https://doi.org/10.1175/JCLI-D-13-00678.1.

——, and Coauthors, 2016: Seasonal forecasts of tropical cyclone activity in a high-atmospheric-resolution coupled prediction system. *J. Climate*, **29**, 1179–1200, https://doi.org/10.1175/JCLI-D-15-0531.1.

Murakami, H., 2014: Tropical cyclones in reanalysis data sets. *Geophys. Res. Lett.*, **41**, 2133–2141, https://doi.org/10.1002/2014GL059519.

NHC, 2018: Costliest U.S. tropical cyclones tables updated. National Hurricane Center, accessed 29 May 2018, 3 pp., https://www.nhc.noaa.gov/news/UpdatedCostliest.pdf.

Reed, A. J., M. E. Mann, K. A. Emanuel, N. Lin, B. P. Horton, A. C. Kemp, and J. P. Donnelly, 2015: Increased threat of tropical cyclones and coastal flooding to New York City during the anthropogenic era. *Proc. Natl. Acad. Sci. USA*, **112**, 12 610–12 615, https://doi.org/10.1073/pnas.1513127112.

Smith, A. B., and R. W. Katz, 2013: US billion-dollar weather and climate disasters: Data sources, trends, accuracy and biases. *Nat. Hazards*, **67**, 387–410, https://doi.org/10.1007/s11069-013-0566-5.

Strachan, J., P. L. Vidale, K. Hodges, M. Roberts, and M.-E. Demory, 2013: Investigating global tropical cyclone activity with a hierarchy of AGCMs: The role of model resolution. *J. Climate*, **26**, 133–152, https://doi.org/10.1175/JCLI-D-12-00012.1.

Swenson, E. T., J. Lu, and D. M. Straus, 2018: Resolution dependence and Rossby wave modulation of atmospheric rivers in and aquaplanet model. *J. Geophys. Res. Atmos.*, **123**, 6297–6311, https://doi.org/10.1029/2017JD027899.

Tartaglione, C. A., S. R. Smith, and J. J. O'Brien, 2003: ENSO impact on hurricane landfall probabilities for the Caribbean. *J. Climate*, **16**, 2925–2931, https://doi.org/10.1175/1520-0442(2003)016<2925:EIOHLP>2.0.CO;2.

Tebaldi, C., B. H. Strauss, and C. E. Zervas, 2012: Modelling sea level rise impacts on storm surges along US coasts. *Environ. Res. Lett.*, **7**, 014032, https://doi.org/10.1088/1748-9326/7/1/014032.

Tolwinski-Ward, S. E., 2015: Uncertainty quantification for a climatology of the frequency and spatial distribution of North Atlantic tropical cyclone landfalls. *J. Adv. Model. Earth Syst.*, **7**, 305–319, https://doi.org/10.1002/2014MS000407.

Van der Paal, B., 2014: A comparison of different methods for modelling rare events data. M.S. Thesis, Faculty of Sciences, Department of Applied Mathematics, Computer Science and Statistics, University of Ghent, 75 pp.

Vecchi, G. A., and Coauthors, 2014: On the seasonal forecasting of regional tropical cyclone activity. *J. Climate*, **27**, 7994–8016, https://doi.org/10.1175/JCLI-D-14-00158.1.

Velden, C., and Coauthors, 2006: The Dvorak tropical cyclone intensity estimation technique: A satellite-based method that has endured for over 30 years. *Bull. Amer. Meteor. Soc.*, **87**, 1195–1210, https://doi.org/10.1175/BAMS-87-9-1195.

Ventrice, M. J., C. D. Thorncroft, and P. E. Roundy, 2011: The Madden–Julian oscillation's influence on African easterly waves and downstream tropical cyclogenesis. *Mon. Wea. Rev.*, **139**, 2704–2722, https://doi.org/10.1175/MWR-D-10-05028.1.

Walsh, K. J. E., M. Fiorino, C. W. Landsea, and K. L. McInnes, 2007: Objectively determined resolution-dependent threshold criteria for the detection of tropical cyclones in climate models and reanalyses. *J. Climate*, **20**, 2307–2314, https://doi.org/10.1175/JCLI4074.1.

Woodruff, J. D., J. L. Irish, and S. J. Camargo, 2013: Coastal flooding by tropical cyclones and sea-level rise. *Nature*, **504**, 44–52, https://doi.org/10.1038/nature12855.

Wu, S.-Y., B. Yarnal, and A. Fisher, 2002: Vulnerability of coastal communities to sea-level rise: A case study of Cape May County, New Jersey, USA. *Climate Res.*, **22**, 255–270, https://doi.org/10.3354/cr022255.

Xiang, B., and Coauthors, 2015: Beyond weather time-scale prediction for Hurricane Sandy and Super Typhoon Haiyan in a Global Climate Model. *Mon. Wea. Rev.*, **143**, 524–535, https://doi.org/10.1175/MWR-D-14-00227.1.

Zhu, J., and Coauthors, 2015: ENSO prediction in Project Minerva: Sensitivity to atmospheric horizontal resolution and ensemble size. *J. Climate*, **28**, 2080–2095, https://doi.org/10.1175/JCLI-D-14-00302.1.